ELSEVIER

Chemical Engineering Journal 141 (2008) 194–203

Chemical Engineering Journal

www.elsevier.com/locate/cej

Enhancement effect of water on oxidation reactions over commercial three-way catalyst

Hyuk Jae Kwon [a], Joon Hyun Baik [a], Yong Tak Kwon [a], In-Sik Nam [a,*], Se H. Oh [b]

[a] *Department of Chemical Engineering/School of Environmental Science and Engineering, Pohang University of Science and Technology (POSTECH), Pohang, Republic of Korea*

[b] *General Motors R&D Planning Center, Warren, MI, USA*

Received 31 July 2007; received in revised form 14 December 2007; accepted 14 December 2007

Abstract

The light-off temperature of the oxidations of CO and C_3H_6 over a commercial three-way catalyst (TWC) was shifted to a lower temperature by the addition of water to the feed stream. From FTIR analysis, the formation of carboxylate and carbonate by a reaction between adsorbed CO and OH on the catalyst surface was observed during the course of the reactions. In addition, the CO desorption peak of CO-TPD shifted to a lower temperature by water, which may be directly indicative of the reduction of the adsorption strength of CO on the catalyst surface. Detailed reaction kinetic models have been developed in view of the concept of microkinetics to describe the effect of water, particularly on the oxidation activity over a commercial TWC.

Keywords: TWC; Oxidation reaction; Enhancement effect of water; TPD; FTIR; Reaction kinetics

1. Introduction

Three-way catalyst (TWC) has been commonly employed for the simultaneous removal of air pollutants by oxidizing carbon monoxide (CO) and hydrocarbons (HCs) and reducing nitrogen oxides (NOx) emitted from gasoline engines [1–4]. Modern commercial three-way catalytic converters typically consist of two monolith bricks of different sizes and catalyst formulations: front and rear bricks containing Pd only and Pt/Rh/Ce catalysts, respectively [1]. The front Pd brick is primarily responsible for controlling CO and HC emissions. On the other hand, residual reactants, especially NOx, are mainly removed over the rear Pt/Rh/Ce brick. However, engine exhaust gas is not only composed of three major air pollutants but also H_2, O_2, H_2O, CO_2 and SO_2. In the exhaust gas composition, water existing up to 10 vol.% also plays an important role as an oxidant, which converts CO and HCs by the water–gas shift (WGS) and the steam reforming (SR) reactions, respectively, especially at high temperature [3,5].

$$\text{CO oxidation} \quad CO + 1/2O_2 \rightarrow CO_2 \tag{1}$$

$$\text{HC oxidation} \quad HCs + O_2 \rightarrow CO_2 + H_2O \tag{2}$$

$$\text{WGS} \quad CO + H_2O \rightarrow CO_2 + H_2 \tag{3}$$

$$\text{SR} \quad HCs + H_2O \rightarrow CO_2 + H_2 \tag{4}$$

As well as its role at high temperature, water can also enhance the oxidation reaction activity of TWC even at low reaction temperature where the WGS and SR reactions are insignificant [6–8]. The reaction kinetics over a ceria promoted Pt–Rh/Al_2O_3 catalyst was developed to describe the promotion of the activity by water at low reaction temperature [7]. However, only the role of the WGS reaction was considered and the model could not account for the enhancement of the catalytic activity, particularly at low reaction temperature where the WGS reaction is not significant. It was also reported that the apparent activation energy of the CO oxidation decreased when water was included in the feed [6]. The alternation of the CO oxidation mechanism in the presence or absence of water was elucidated by the compensation effect [8]. Although the role of water at low

* Corresponding author. Tel.: +82 54 279 2264; fax: +82 54 279 8299.
E-mail address: isnam@postech.ac.kr (I.-S. Nam).

1385-8947/$ – see front matter © 2007 Elsevier B.V. All rights reserved.
doi:10.1016/j.cej.2007.12.017

Nomenclature

C_i	concentration of i species (mol/m^3)
C_i^0	initial concentration of i species (mol/m^3)
$E_{a,i}$	activation energy of i species (J/mol)
ΔH_i	heat of adsorption of i species (J/mol)
k_i	rate coefficient for a reaction (m^3/mol s)
$k_{0,i}$	frequency factor of rate coefficient for a reaction (m^3/mol s)
K_i	equilibrium constants (m^3/mol)
$K_{0,i}$	pre-exponential factor of equilibrium constants (m^3/mol)
r_i	reaction rate for the i species based on catalytic volume (mol/m^3 s)
S	active surface reaction site
X_i	fractional conversion of i species

Greek letters

θ_i	surface coverage of i species
τ	reactor space time (residence time) of the feed as stream (s)

temperature for the enhancement of the CO oxidation activity has been generally recognized as a modification of the catalyst surface and/or the reduction of the self-poisoning of CO, it has not been systematically examined yet, particularly in the low reaction temperature region near the light-off temperature of TWC.

In the present study, the CO oxidation and simultaneous CO and C_3H_6 oxidation activities with and without water in the feed were investigated to understand the enhancement effect of water on the oxidation reactions at low reaction temperature. Although TWC converters are composed of two bricks as mentioned, Pd catalyst has been employed since the oxidation reactions mainly occur in the front brick more actively. To confirm the adsorption strength and verify the reaction intermediates, we performed catalyst characterization including TPD and FTIR. In addition, H_2-TPR study was also conducted to confirm the active reaction site of the present catalytic system. Finally, a detailed reaction kinetic model was developed in view of microkinetics to systematically describe the enhancement effect of water on the TWC activity.

2. Experimental

2.1. Catalyst preparation

A commercial three-way monolith brick mainly containing Pd was obtained from General Motors. The entire catalyst brick including cordierite was crushed, mixed and pelletized into 20/30-mesh size to reduce and avoid heat of reaction and mass transfer resistance. For the FTIR analysis, the washcoat layer on the channels of the monolith was scraped off from the monolith sample. The physicochemical properties of the catalyst samples are listed in Table 1.

Table 1
Physicochemical properties of the commercial Pd catalyst prepared

Catalyst	Pd content (wt.%)	BET surface area (m^2/g)
A	0.97	43
B	3.03	196

A: washcoat + cordierite mixture; B: washcoat scraped off from the monolith brick.

2.2. Reactor system and experimental procedure

The TWC activity of a commercial Pd catalyst was examined by using a packed bed U tube type integral reactor immersed in a molten-salt bath to maintain the isothermal condition of the catalyst bed [9–11]. One gram of the catalyst powder of 20/30-mesh size was charged into the reactor to minimize the mass transfer limitations of the catalyst. The activity was examined under steady-state conditions in the temperature range from 150 to 350 °C. The difference of the temperature between top and bottom of the catalyst bed was controlled within 2 °C. In order to develop the reaction kinetics in view of the microkinetics, the TWC activity was examined by changing the reactor space velocities (SV) from 100,000 to 300,000 h^{-1} under the following feed containing 10 vol.% CO_2 and Ar balance: (i) 1 vol.% CO and 0.5 vol.% O_2, (ii) 1 vol.% CO, 500 ppm C_3H_6 and 1 vol.% O_2, (iii) 1 vol.% CO, 500 ppm C_3H_6, 1 vol.% O_2 and 10 vol.% H_2O, and (iv) 1 vol.% CO, 0.5 vol.% O_2 and 10 vol.% H_2O. The catalyst was pretreated under a stoichiometric feed condition containing 0.9 vol.% CO, 0.6 vol.% O_2, 0.3 vol.% H_2, 10 vol.% CO_2 and 10 vol.% H_2O at 450 °C for 2 h and then cooled in Ar atmosphere to the desired temperature. The concentrations of CO, C_3H_6, CO_2 and O_2 were analyzed by on-line gas chromatography (GC) equipped with TCD and FID (Agilent, model 6890N). Ar was used as a balance gas to analyze the H_2 formation during the course of the WGS and SR reactions over TWC when water exists in the feed.

2.3. Catalyst characterization

BET surface area was measured by Micromeritics ASAP 2010 sorption analyzer with a static volumetric technique based on the amount of N_2 adsorbed at liquid N_2 temperature.

CO-TPD (temperature programmed desorption) was performed in a quartz U tube reactor containing 0.2 g of the catalyst powder. The TPD run was started from room temperature to 800 °C, and the desorbed molecules from the catalyst were monitored by an on-line mass spectrometer (Pfeiffer Vacuum, GMG 422I).

An FTIR analysis of the reaction intermediating species adsorbed on the catalyst surface under in situ conditions at 175 °C was performed with an M2000 spectrometer (MIDAC Corporation). The spectra were taken in the range 400–4000 cm^{-1} with a resolution of 2 cm^{-1}. The spectrum was taken after the sample was exposed to each of the following gaseous environments for 1 h by adding and removing the gas component in the feed as follows: (a) 1 vol.% CO, (b) 1 vol.%

Table 2
Light-off temperatures of the oxidation reaction

Reactions		T_{50} (°C)	
		CO	C_3H_6
CO oxidation (Fig. 1)	w/o H_2O	180	–
	w/H_2O	169	–
C_3H_6 oxidation (Fig. 1)	w/o H_2O	–	190
	w/H_2O	–	190
CO and C_3H_6 oxidations (Fig. 2)	w/o H_2O	208	209
	w/H_2O	203	204

CO and 1 vol.% O_2, (c) 1 vol.% CO, 1 vol.% O_2, and 10 vol.% H_2O, (d) 1 vol.% CO and 10 vol.% H_2O, and (e) 10 vol.% H_2O.

H_2-TPR (temperature programmed reduction) was performed using 0.2 g of the catalyst heated at 10 °C/min under hydrogen atmosphere (5% in Ar) at a flow rate of 30 ml/min. The catalyst was pretreated in air at 500 °C for 2 h prior to TPR. A thermal conductivity detector (TCD; HP 5890 GC) was employed to monitor the consumption of hydrogen by the reduction of the catalyst. The effluent stream was dried in a cold trap prior to reaching TCD of GC.

3. Results and discussion

3.1. Effect of water on the oxidation reactions

The activity of the Pd catalyst for CO oxidation with and without water vapor as a function of the reaction temperature can be observed in Fig. 1(a). When the feed gas stream does not contain water vapor, the light-off temperature of CO ($T_{50,CO}$) is 180 °C, as listed in Table 2. The catalytic activity of the CO oxidation in the presence of 10 vol.% water shifts to the lower reaction temperature ($T_{50,CO}$ = 169 °C). It clearly shows that water can enhance the CO oxidation reaction even at low reaction temperature. On the other hand, the addition of water to the feed stream hardly alters the C_3H_6 oxidation activity, as shown in Fig. 1(b). Therefore, the adsorption characteristics of C_3H_6 on the catalyst may be hardly affected by water. For the simultaneous oxidations of CO and C_3H_6, the enhancement effect of water can also be observed, as shown in Fig. 2. When water was included in the feed stream, both light-off temperatures of CO and C_3H_6 also slightly decreased from 208 and 209 °C to 204 and 203 °C, respectively. The simultaneous oxidation was enhanced by the presence of water, probably due to the alteration of the adsorption characteristics of CO on the catalyst surface.

To confirm the possibility of the occurrence of WGS and SR reactions at low reaction temperature, both reactions were examined without O_2 in the feed. As shown in Fig. 3, the WGS and SR reactions begin around 275 °C and the conversion of their activities reaches 46 and 87% around 400 °C, respectively. Moreover, a significant amount of H_2 was observed as the conversions of CO and C_3H_6 increased. Therefore, the enhancement effect of

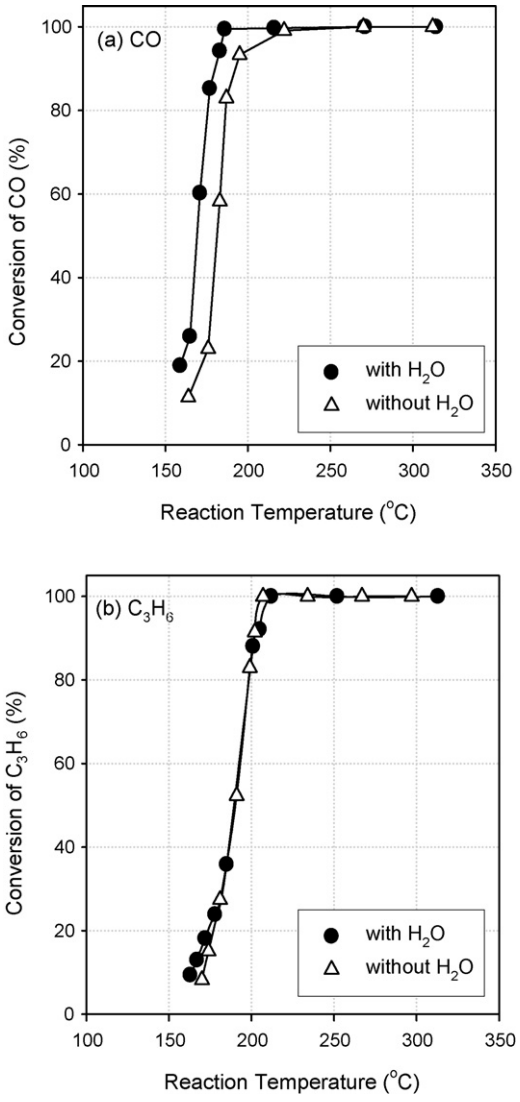

Fig. 1. Effect of water on the oxidation activities of CO and C_3H_6 over the commercial Pd catalyst. Feed gas composition: (a) 1 vol.% CO, 0.5 vol.% O_2 and (b) 500 ppm C_3H_6, 1 vol.% O_2 with 10 vol.% CO_2, 0 or 10 vol.% H_2O and Ar balance; reactor SV: 100,000 h^{-1}.

water on the oxidation reactions at low reaction temperature, particularly near the light-off point of TWC, is not mainly due to the WGS and SR reactions as commonly speculated [6–8].

3.2. Catalyst characterization

3.2.1. Temperature programmed desorption (TPD) of CO

To confirm the cause of the water enhancement effect at low reaction temperature, CO-TPD was examined. Fig. 4 shows the effect of water on the CO adsorption characteristics on the surface of the Pd catalyst. The desorption peaks at around 100 °C are probably due to the weakly adsorbed CO on Al_2O_3, the catalyst support in the present catalytic system [12,13]. On the other hand, the main desorption peak of CO shifts to a lower temperature from 320 to 265 °C when water is present in the feed. The shift of the CO desorption temperature in the presence of water suggests that water may reduce the CO adsorption strength and

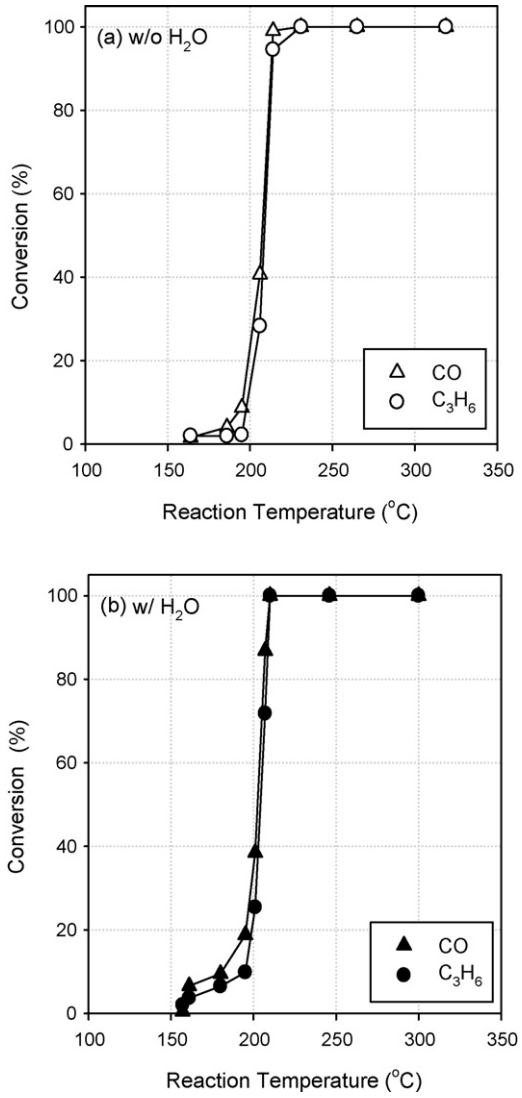

Fig. 2. Effect of water on CO and C_3H_6 oxidation activities over the commercial Pd catalyst. (a) w/o H_2O and (b) w/H_2O. Feed gas composition: 1 vol.% CO, 500 ppm C_3H_6, 1 vol.% O_2, 10 vol.% CO_2, 0 or 10 vol.% H_2O and Ar balance; reactor SV: 100,000 h^{-1}.

it may be responsible for the enhancement of low temperature CO oxidation activity [6–8].

3.2.2. *In situ FTIR analysis*

Fig. 5(A) shows the IR spectra in the range of 2500–1700 cm^{-1} under in situ condition at 175 °C to elucidate the role of water at low reaction temperature. As shown in Fig. 5(A), two types of carbonyl species are observed. One of them is at around 2070 cm^{-1} of IR band, which may be assigned to atop the (linear) carbonyl species chemisorbed on metallic palladium particles [14–17]. The other is a peak appearing at around 1970 cm^{-1}, which can be attributed to carbonyl species chemisorbed on the bridging sites [14–16]. The IR peak intensity of carbonyl species, particularly the bridged carbonyls on Pd at 1970 cm^{-1}, decreases and becomes broader when water is included in the feed, which may indicate a moderation of the self-poisoning of CO on the active reaction sites of the catalyst.

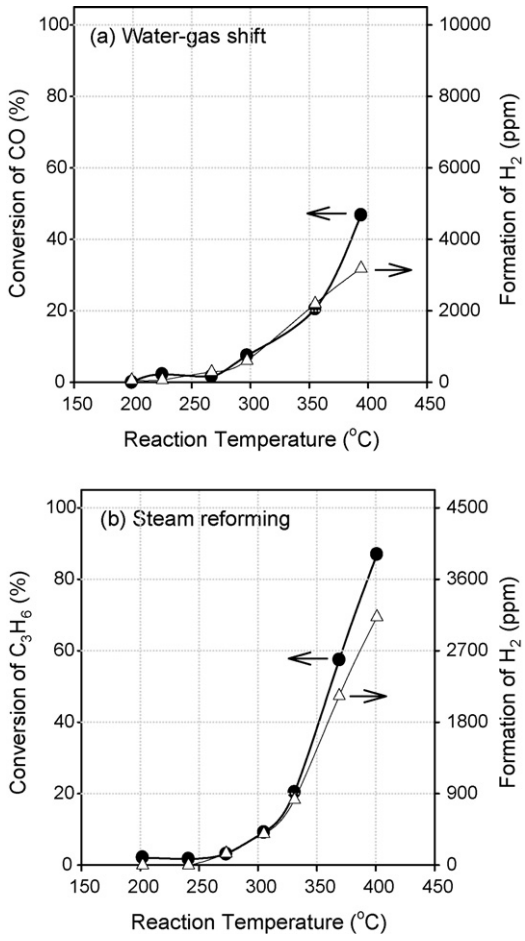

Fig. 3. Activities of (a) WGS and (b) SR reactions over the commercial Pd catalyst. Feed gas composition: 1 vol.% CO or 500 ppm C_3H_6, 10 vol.% CO_2, 10 vol.% H_2O and Ar balance; reactor SV: 100,000 h^{-1}.

Fig. 5(B) shows the detailed spectra in the range from 4000 to 3200 cm^{-1} of FTIR wave number. As expected, a broad hydroxyl band appears around 3565 cm^{-1} when water is included in the feed (c–e). The adsorption of water on the

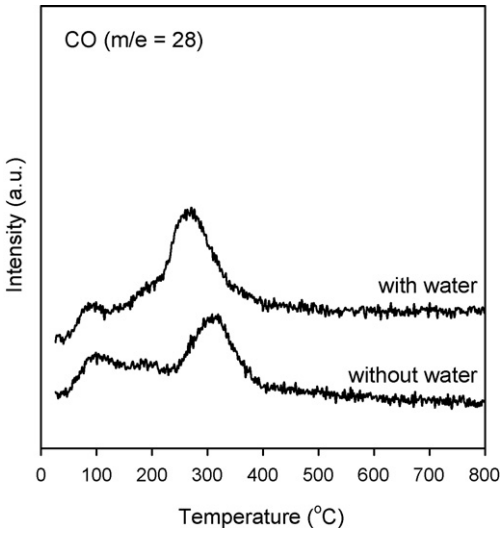

Fig. 4. CO-TPD profile for CO (m/e = 28) over the commercial Pd catalyst. (a) w/H_2O and (b) w/o H_2O.

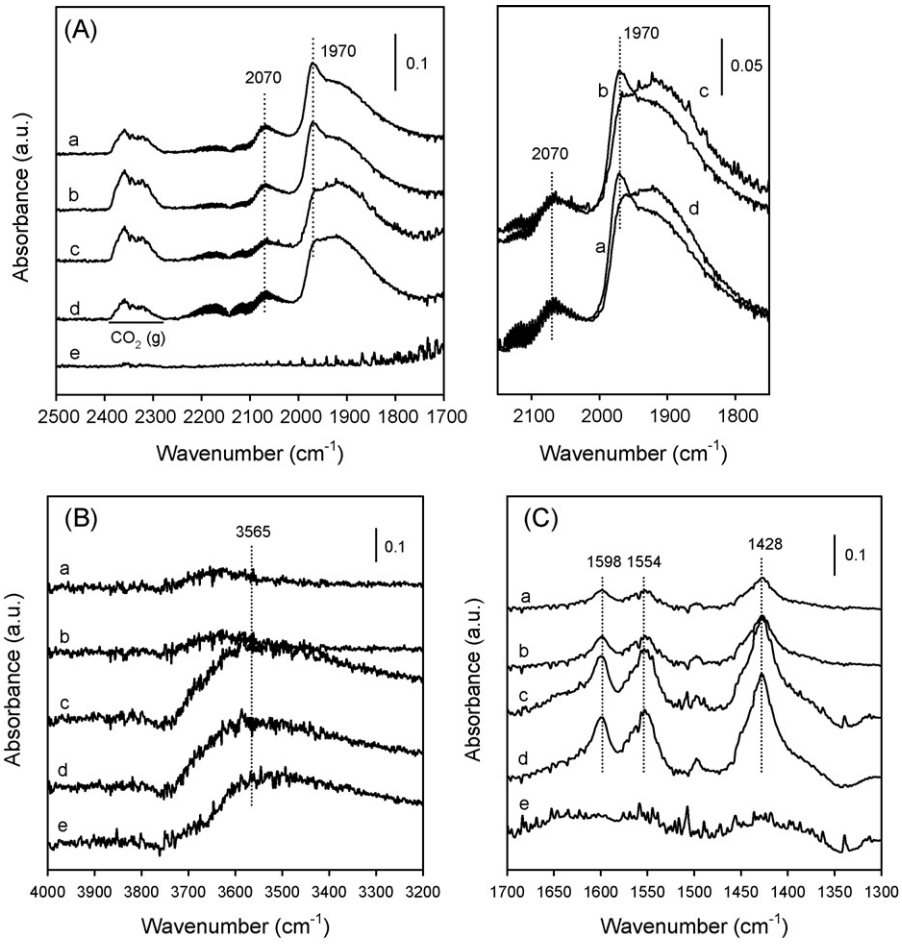

Fig. 5. FTIR spectra of CO adsorbed over the commercial Pd catalyst under in situ sequential feed flow. (A) Carbonyl species, (B) OH-stretching and (C) surface carboxylate and carbonate species vibration region. Sequential feed gas composition: (a) 1 vol.% CO, (b) 1 vol.% CO and 1 vol.% O_2, (c) 1 vol.% CO, 1 vol.% O_2, and 10 vol.% H_2O, (d) 1 vol.% CO and 10 vol.% H_2O, and (e) 10 vol.% H_2O at 175 °C.

catalyst surface can be expressed in the following ways [18]:

$$H_2O + S \leftrightarrow H_2O^{\bullet}S \quad (5)$$

$$H_2O^{\bullet}S + S \rightarrow H^{\bullet}S + OH^{\bullet}S \quad (6)$$

$$H_2O^{\bullet}S + O^{\bullet}S \rightarrow 2OH^{\bullet}S \quad (7)$$

A carboxylate and carbonate vibration region (1700–1300 cm^{-1}) has been particularly observed as shown in Fig. 5(C). The peak at 1428 cm^{-1} is attributed to carbonate species formed during the course of the reaction [14,19]. The bands within the range from 1650 to 1500 cm^{-1} can be assigned to carboxylate species formed on Pd [19]. In the presence of water in the feed (c and d), the band intensities of both species are increased, as shown in Fig. 5(C). The formation of these apparent carboxylate species on the catalyst surface when both CO and water exist in the feed can be explained by reactions (8) to (10) between adsorbed CO and OH formed through the reactions (6) and (7):

$$CO^{\bullet}S + OH^{\bullet}S \rightarrow COO^{\bullet}S + H^{\bullet}S \quad (8)$$

$$CO^{\bullet}S + OH^{\bullet}S \rightarrow COOH^{\bullet}S + S \quad (9)$$

$$COOH^{\bullet}S + S \rightarrow COO^{\bullet}S + H^{\bullet}S \quad (10)$$

This result is also quite consistent with those of Mhadeshwar and Vlachos [18] and Bergeld et al. [20]. They discussed that the adsorbed water promoted CO oxidation reaction at low temperature by both the direct (reaction (8)) and indirect (reactions (9) and (10)) pathways and concluded that $OH^{\bullet}S$ played an autocatalytic role for the low temperature CO oxidation reaction through the above reactions (8) to (10). Therefore, it reveals that the formation of the reaction intermediates, including carboxylate and carbonate, is critical for enhancing the CO oxidation reaction over the TWC by water.

3.2.3. *Temperature programmed reduction (TPR) of H_2*

Fig. 6 shows the H_2-TPR profile of the Pd only catalyst employed in the present study. H_2-TPR was conducted under H_2 (5% in Ar) in the temperature range from RT to 700 °C after the catalyst pretreatment with air. The Pd catalyst shows a large single peak in the temperature range of 100–150 °C (characteristic of bulk Pd oxide of the metal crystallites due to the pretreatment) [21,22]. This result indicates that Pd is the primary active reaction site and no interaction with the support has been observed. Manuel et al. reported that the reduced noble metal had been confirmed as a unique active reaction site over the single crystal or silica- and alumina-supported metal catalysts including

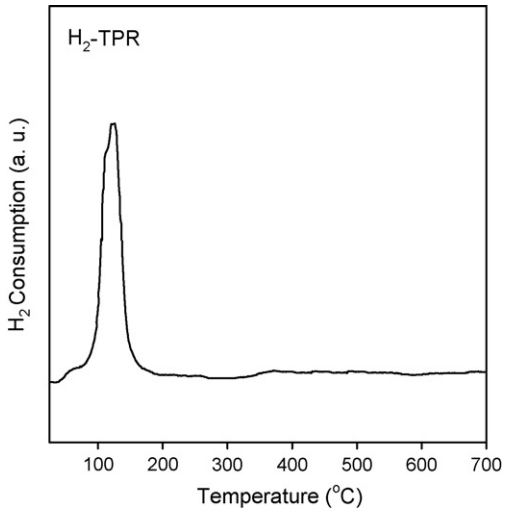

Fig. 6. H_2-TPR profile of the commercial Pd catalyst.

Pd [23]. Iglesias-Juez et al. also reported that the Pd existed in metallic state, zero-valent Pd and Pd(I) and Pd(II) were hardly effective for CO oxidation [24].

3.3. Development of reaction kinetics

3.3.1. Detailed reaction kinetics

From the CO-TPD and FTIR studies, the reaction kinetics can be deduced to describe the enhancement effect of water on the TWC activity over the commercial Pd catalyst. In the present study, a detailed kinetic model has been systematically developed in view of the microkinetics. It should be noted that the feature of the present approach might be the utilization of the identical kinetic parameters calculated from a series of experimental kinetic data observed under the sequential inclusion of each gaseous component into the feed for probably describing the microkinetic performance to confirm the effect of water on the oxidation reactions of CO and C_3H_6. Metallic Pd is a unique active reaction site as confirmed by H_2-TPR.

The reaction kinetics has been developed on the basis of the following assumptions: (i) all reaction steps are assumed to be a non-elementary, mainly first-order reaction with respect to each of the reactants involved, (ii) all reactants except CO_2 adsorb on the catalyst surface, (iii) oxygen adsorbs dissociatively on the catalyst surface, and (iv) the surface reaction is a rate-determining step that is described by a competitive dual-site Langmuir–Hinshelwood mechanism, and (v) all "S" is the identical reaction site, metallic Pd [7,9,18,25,26,28].

3.3.1.1. CO oxidation reaction. Based upon the assumption, the reaction mechanism when CO and O_2 only exist in the feed can be described by the following reaction steps.

Reactant adsorption and desorption:

$$CO + S \leftrightarrow CO^{\bullet}S \qquad K_1 \qquad (11)$$

$$O_2 + 2S \leftrightarrow 2O^{\bullet}S \qquad K_2 \qquad (12)$$

Surface reactions:

$$r_1 \quad CO^{\bullet}S + O^{\bullet}S \rightarrow CO_2 + 2S \qquad k_1 \qquad (13)$$

where S is surface reaction site, and K_i and k_i are the adsorption equilibrium and surface reaction rate constants, respectively. The rate expression can be derived by using the Hougen–Watson formalism. The steady-state rate equations can be simply expressed as follows.

For CO consumption,

$$r_{CO} = \frac{dX_{CO}}{d\tau} = r_1 = \frac{1}{D^2}[k_1 K_1 K_2 C_{O_2}^0 (1 - X_{CO})(1 - X_{O_2})] \qquad (14)$$

For O_2 consumption,

$$r_{O_2} = \frac{dX_{O_2}}{d\tau} = 0.5 r_1 = \frac{0.5}{D^2}[k_1 K_1 K_2 C_{CO}^0 (1 - X_{CO})(1 - X_{O_2})] \qquad (15)$$

From the site balance, D can be obtained as follows:

$$1 = \theta_v + \theta_{CO} + \theta_O$$

$$\theta_v = \frac{1}{D}$$

$$D = 1 + K_1 C_{CO}^0 (1 - X_{CO}) + K_2 C_{O_2}^0 (1 - X_{O_2}) \qquad (16)$$

3.3.1.2. Simultaneous CO and C_3H_6 oxidation reactions. For the simultaneous oxidations of CO and C_3H_6, the additional reactions related to C_3H_6 are also considered for the following reaction steps and the rate equations are derived by the identical method as discussed.

Reactant adsorption and desorption:

$$CO + S \leftrightarrow CO^{\bullet}S \qquad K_1 \qquad (11)$$

$$O_2 + 2S \leftrightarrow 2O^{\bullet}S \qquad K_2 \qquad (12)$$

$$C_3H_6 + S \leftrightarrow C_3H_6{}^{\bullet}S \qquad K_3 \qquad (17)$$

Surface reactions:

$$r_1 \quad CO^{\bullet}S + O^{\bullet}S \rightarrow CO_2 + 2S \quad k_1 \qquad (13)$$

$$r_2 \quad C_3H_6{}^{\bullet}S + 9O^{\bullet}S \rightarrow 3CO_2 + 3H_2O^{\bullet}S + 7S \quad k_2 \qquad (18)$$

The steady-state rate equations can be expressed as follows:

For CO consumption,

$$r_{CO} = \frac{dX_{CO}}{d\tau} = r_1 = \frac{1}{D^2}[k_1 K_1 K_2 C_{O_2}^0 (1 - X_{CO})(1 - X_{O_2})] \qquad (19)$$

For C_3H_6 consumption,

$$r_{C_3H_6} = \frac{dX_{C_3H_6}}{d\tau} = r_2 = \frac{1}{D^2}[k_2 K_2 K_3 C_{O_2}^0 (1 - X_{C_3H_6})(1 - X_{O_2})] \qquad (20)$$

For O_2 consumption,

$$r_{O_2} = \frac{dX_{O_2}}{d\tau} = 0.5r_1 + 4.5r_2 = \frac{1}{D^2}[0.5k_1K_1K_2C^0_{CO}(1-X_{CO})(1-X_{O_2}) + 4.5k_2K_2K_3C^0_{C_3H_6}(1-X_{C_3H_6})(1-X_{O_2})] \quad (21)$$

From the site balance, D can be obtained as follows:

$$1 = \theta_v + \theta_{CO} + \theta_{C_3H_6} + \theta_O$$

$$\theta_v = \frac{1}{D}$$

$$D = 1 + K_1C^0_{CO}(1-X_{CO}) + K_2C^0_{O_2}(1-X_{O_2}) + K_3C^0_{C_3H_6}(1-X_{C_3H_6}) \quad (22)$$

3.3.1.3. Simultaneous CO and C_3H_6 oxidation reactions in the presence of water. To elucidate the effect of water on the activity for the simultaneous CO and C_3H_6 oxidation reactions, the surface reaction mechanism and the rate equations have been derived.

Reactant adsorption and desorption:

$$CO + S \leftrightarrow CO^{\bullet}S \quad K_1 \quad (11)$$

$$O_2 + 2S \leftrightarrow 2O^{\bullet}S \quad K_2 \quad (12)$$

$$C_3H_6 + S \leftrightarrow C_3H_6{}^{\bullet}S \quad K_3 \quad (17)$$

$$H_2O + S \leftrightarrow H_2O^{\bullet}S \quad K_4 \quad (5)$$

Surface reactions:

$$r_1 \quad CO^{\bullet}S + O^{\bullet}S \rightarrow CO_2 + 2S \quad k_1 \quad (13)$$

$$r_2 \quad C_3H_6{}^{\bullet}S + 9O^{\bullet}S \rightarrow 3CO_2 + 3H_2O^{\bullet}S + 7S \quad k_2 \quad (18)$$

$$r_3 \quad H_2O^{\bullet}S + S \rightarrow H^{\bullet}S + OH^{\bullet}S \quad k_3 \quad (6)$$

$$r_4 \quad H_2O^{\bullet}S + O^{\bullet}S \rightarrow 2OH^{\bullet}S \quad k_4 \quad (7)$$

$$r_5 \quad H^{\bullet}S + O^{\bullet}S \rightarrow OH^{\bullet}S + S \quad k_5 \quad (23)$$

$$r_6 \quad CO^{\bullet}S + 2OH^{\bullet}S \rightarrow CO_2 + H_2O^{\bullet}S + 2S \quad k_6 \quad (24)$$

Reaction (24) has been included to describe the enhancement effect of water, which implies the reactions (8)–(10) as confirmed by FTIR analysis.

Similar to the approach employed by Oh et al. [26], Cho [27] and Hoebink et al. [28], θ_H and θ_{OH} can be described on the basis of the steady-state conversion equations as follows:

$$\theta_H : r_3 - r_5 = 0$$

$$\theta_H = \frac{k_3K_4C_{H_2O}}{k_5K_2C_{O_2}}\theta_v \quad (25)$$

$$\theta_{OH} : r_3 + 2r_4 + r_5 - 2r_6 = 0$$

$$\theta_{OH} = \frac{k_3K_4C_{H_2O} + k_4K_2K_4C_{O_2}C_{H_2O}}{k_6K_1C_{CO}}\theta_v \quad (26)$$

The steady-state rate equations can be expressed as follows:
For CO consumption,

$$r_{CO} = \frac{dX_{CO}}{d\tau} = r_1 + r_6 = \frac{1}{D^2}[k_1K_1K_2C^0_{O_2}(1-X_{CO})(1-X_{O_2}) + (k_3 + k_4K_2C^0_{O_2}(1-X_{O_2}))K_4C^0_{H_2O}/C^0_{CO}] \quad (27)$$

For C_3H_6 consumption,

$$r_{C_3H_6} = \frac{dX_{C_3H_6}}{d\tau} = r_2 = \frac{1}{D^2}[k_2K_2K_3C^0_{O_2}(1-X_{C_3H_6})(1-X_{O_2})] \quad (28)$$

For O_2 consumption,

$$r_{O_2} = \frac{dX_{O_2}}{d\tau} = 0.5r_1 + 4.5r_2 + 0.5r_4 + 0.5r_5 = \frac{1}{D^2}[0.5(k_1K_1K_2C^0_{CO}(1-X_{CO})(1-X_{O_2}) + k_4K_2K_4C^0_{H_2O}(1-X_{O_2}) + k_3K_4C^0_{H_2O}/C^0_{O_2}) + 4.5k_2K_2K_3C^0_{C_3H_6} \times (1-X_{C_3H_6})(1-X_{O_2})] \quad (29)$$

It has been assumed that the concentration of water, $C_{H_2O,}$ is constant due to the high feed concentration of water (10 vol.%) compared to the rest of the gas composition employed in the present study ($C_{H_2O} = C^0_{H_2O}$). From the site balance, D can be obtained as follows:

$$1 = \theta_v + \theta_{CO} + \theta_{C_3H_6} + \theta_O + \theta_{H_2O} + \theta_H + \theta_{OH}$$

$$\theta_v = \frac{1}{D}$$

$$D = 1 + K_1C^0_{CO}(1-X_{CO}) + K_2C^0_{O_2}(1-X_{O_2}) + K_3C^0_{C_3H_6}(1-X_{C_3H_6}) + K_4C^0_{H_2O} + \frac{k_3K_4C^0_{H_2O}}{k_5K_2C^0_{O_2}(1-X_{O_2})} + \frac{(k_3 + k_4K_2C^0_{O_2}(1-X_{O_2}))K_4C^0_{H_2O}}{k_6K_1C^0_{CO}(1-X_{CO})} \quad (30)$$

3.3.2. Parameter estimation

The parameters of the proposed detailed reaction kinetic expressions were estimated by comparing the model prediction of CO and C_3H_6 conversions with the experimental data

measured in the present study. The kinetic parameters obtained from the literature [5,6,29–31] were employed as initial guesses for the parameter estimation. The nonlinear ordinary differential equations were solved by Gear's method, which can handle any degree of stiffness of the gradients for the model equations while allowing the desired accuracy of integration with moderate computing time. The parameters were estimated by using nonlinear regression to minimize the sum of squares of the difference between the experimental and calculated data. A regression routine for the minimization uses the Marquardt algorithm [32].

$$\text{minimize} \sum_{i=0}^{n} (X_i^{\text{exp}} - X_i^{\text{cal}})^2 \tag{31}$$

The computer subroutine program for the estimation of the parameters was prepared by using MATLAB® (version 6.1, The MathWorks Inc.).

3.3.3. Model prediction

Fig. 7 shows the model prediction for the CO oxidation reaction by the rate Eqs. (14)–(16). The model well predicts the experimental data over the commercial Pd catalyst at various reactor space velocities from 100,000 to 300,000 h^{-1}. With the identical kinetic parameters obtained from the kinetic study for

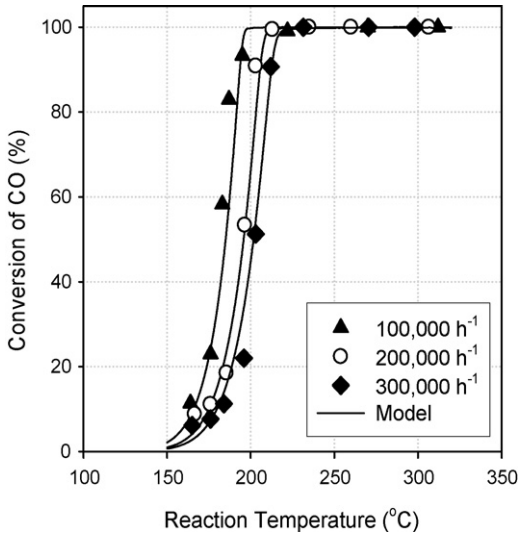

Fig. 7. Comparison of predicted and measured CO conversion on the CO oxidation reaction over the commercial Pd catalyst. Feed gas composition: 1 vol.% CO, 0.5 vol.% O_2, 10 vol.% CO_2 and Ar balance; reactor SV: 100,000–300,000 h^{-1}.

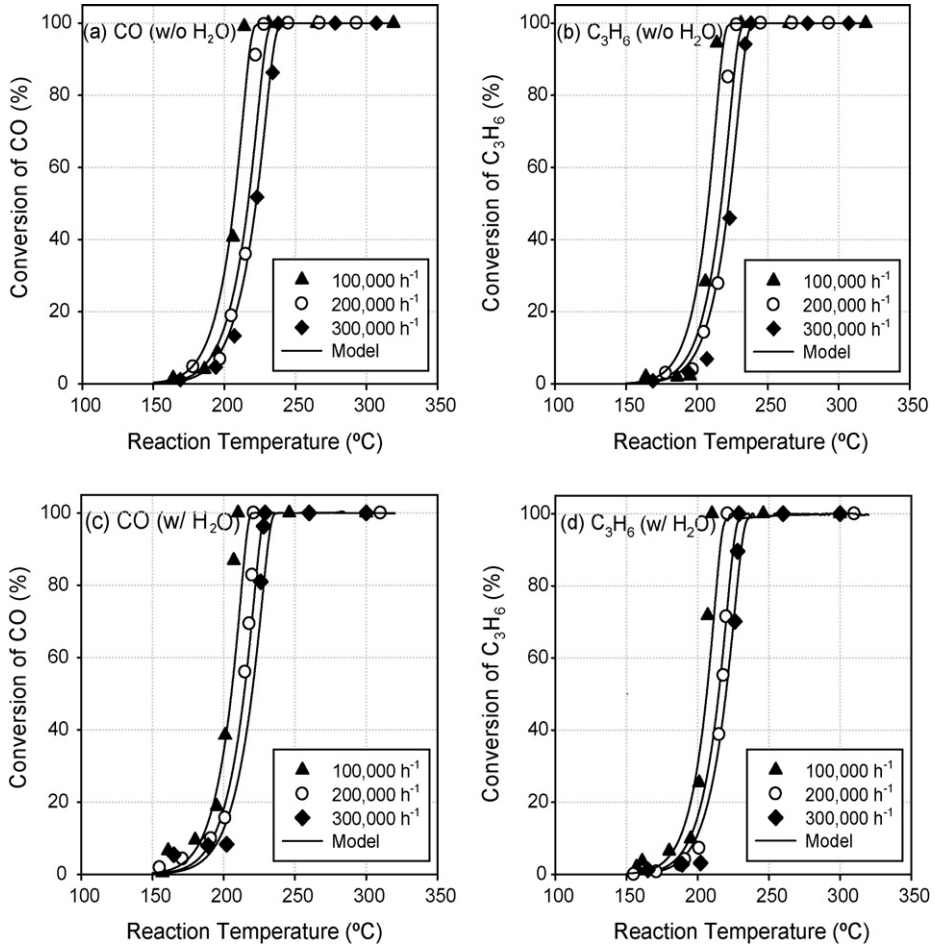

Fig. 8. Comparison of predicted and measured CO and C_3H_6 conversions over the commercial Pd catalyst. (a) CO and (b) C_3H_6 (w/o water), (c) CO and (d) C_3H_6 (w/water). Feed gas composition: 1 vol.% CO, 500 ppm C_3H_6, 1 vol.% O_2, 10 vol.% CO_2, 0 or 10 vol.% H_2O and Ar balance; reactor SV: 100,000–300,000 h^{-1}.

Table 3
Kinetic parameters estimated from the experimental data over the commercial Pd catalyst

Kinetic parameters[a]			
$K_{0,1}$	2.0×10^{-3}	ΔH_1	38
$K_{0,2}$	7.0×10^{-8}	ΔH_2	83
$K_{0,3}$	4.1×10^{-3}	ΔH_3	43
$K_{0,4}$	5.5×10^{-9}	ΔH_4	42
$k_{0,1}$	2.2×10^{3}	$E_{a,1}$	127
$k_{0,2}$	3.2×10^{4}	$E_{a,2}$	144
$k_{0,3}$	1.2×10^{2}	$E_{a,3}$	121
$k_{0,4}$	1.9×10^{4}	$E_{a,4}$	108
$k_{0,5}$	8.7×10^{3}	$E_{a,5}$	55
$k_{0,6}$	3.8×10^{-1}	$E_{a,6}$	82

[a] $K_{0,i}$ (m^3/mol), $k_{0,i}$ (m^3/mol s), ΔH_i (kJ/mol) and $E_{a,i}$ (kJ/mol).

CO and O_2 system, model prediction for the simultaneous oxidation reactions of CO and C_3H_6 was performed by using Eqs. (19)–(22). As shown in Fig. 8(a) and (b), the light-off behavior of both CO and C_3H_6 oxidation reactions has been well described by the model developed. Moreover, the model reasonably predicts the water enhancement effect on the oxidation reactions at low reaction temperature even with the identical kinetic parameters of the rate Eqs. (27)–(30), as shown in Fig. 8(c) and (d). The estimated kinetic parameters are listed in Table 3.

The activation energies, $E_{a,1}$ and $E_{a,2}$ for the oxidation reactions of CO and C_3H_6 are 127 and 144 kJ/mol, respectively. Based upon the results from CO-TPD and FTIR, the reaction pathway of the water enhancement effect on the CO oxidation reaction, reaction (24), was included for developing the kinetic model in the present study. The activation energy, $E_{a,6}$ of the reaction between CO and OH over the reaction (24), however, is 82 kJ/mol. It is smaller than that of the CO oxidation reaction (13), 127 kJ/mol, which is quite reasonable for elucidating the enhancement effect of water. It may simply reveal that the kinetic model developed on the basis of the microkinetic reaction pathway employed in the present study to describe the enhancement effect of water may be quite appropriate for predicting the oxidation reactions of CO and C_3H_6 over commercial TWC.

To confirm the detailed reaction kinetics developed in view of microkinetics, a kinetic model for CO oxidation reaction when water exists in the feed was developed to independently predict the experimental results with the identical parameters obtained from the microkinetic study. Since C_3H_6 was not included in the feed, the reaction (18) was eliminated from the model for the simultaneous CO and C_3H_6 oxidation reactions, Eqs. (27)–(30), and then the steady-state rate equations can be obtained as follows:

For CO consumption,

$$r_{CO} = \frac{dX_{CO}}{d\tau} = r_1 + r_6 = \frac{1}{D^2}[k_1 K_1 K_2 C^0_{O_2}(1 - X_{CO})(1 - X_{O_2}) + (k_3 + k_4 K_2 C^0_{O_2}(1 - X_{O_2}))K_4 C^0_{H_2O}/C^0_{CO}] \quad (32)$$

For O_2 consumption,

$$r_{O_2} = \frac{dX_{O_2}}{d\tau} = 0.5r_1 + 0.5r_4 + 0.5r_5 = \frac{0.5}{D^2}[(k_1 K_1 K_2 C^0_{CO}(1 - X_{CO})(1 - X_{O_2}) + k_4 K_2 K_4 C^0_{H_2O}(1 - X_{O_2}) + k_3 K_4 C^0_{H_2O}/C^0_{O_2})] \quad (33)$$

From the site balance, D can be obtained as follows:

$$D = 1 + K_1 C^0_{CO}(1 - X_{CO}) + K_2 C^0_{O_2}(1 - X_{O_2}) + K_4 C^0_{H_2O} + \frac{k_3 K_4 C^0_{H_2O}}{k_5 K_2 C^0_{O_2}(1 - X_{O_2})} + \frac{(k_3 + k_4 K_2 C^0_{O_2}(1 - X_{O_2}))K_4 C^0_{H_2O}}{k_6 K_1 C^0_{CO}(1 - X_{CO})} \quad (34)$$

Fig. 9 compares the model prediction with the identical kinetic parameters listed in Table 3 to the experimental data for the CO oxidation reaction with water in the feed. Based on Eqs. (32)–(34), the kinetic model well predicts and describes the CO conversion as well as the water enhancement effect even when C_3H_6 does not exist in the feed. Therefore, the parameters estimated from the model developed can be considered as reasonable values over the Pd catalyst employed in the present study. Consequently, a detailed kinetic model developed in the present study is quite adequate for predicting the enhancement effect of water on the oxidation reactions, particularly at low reaction temperature.

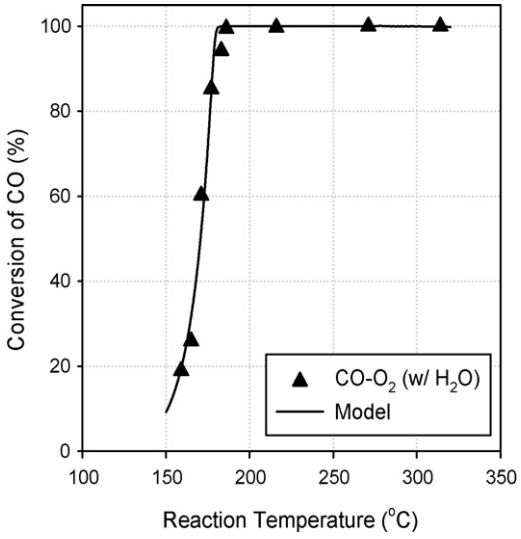

Fig. 9. Comparison of predicted and measured CO conversion for verifying the kinetic parameters on the CO oxidation reaction including water over the commercial Pd catalyst. Feed gas composition: 1 vol.% CO, 0.5 vol.% O_2, 10 vol.% CO_2, 10 vol.% H_2O and Ar balance; reactor SV: 100,000 h^{-1}.

4. Conclusions

The light-off temperature of the CO oxidation reaction and simultaneous oxidation reactions of CO and C_3H_6 shifted to a lower temperature by the addition of water to the feed stream, even in the range of the reaction temperature where the WGS and SR reactions hardly occur. From the systematic CO-TPD and in situ FTIR studies, the reaction between CO and OH from water adsorbed onto the catalyst surface mainly occurs through the formation of a reaction intermediate such as carboxylate and carbonate, which may be direct evidence for clarifying the activity enhancement of the oxidation reaction by water at low reaction temperature. Detailed kinetic models have been derived in view of microkinetics without the lumped kinetic parameters commonly employed for the development of the reaction kinetics. Furthermore, the detailed models developed by sequential addition of the feed gas components, such as CO, C_3H_6 and H_2O, are able to quantify the water enhancement effect at low reaction temperature. Therefore, the reaction kinetics developed in the present study for describing the water enhancement effect on the oxidation reactions may provide useful information for deriving the realistic complex reaction kinetics under real world operating conditions over commercial TWC.

Acknowledgements

Financial support of this work was provided by GM (1KI0440101) and the National Research Laboratory Program (ROA-2007-000-20050-0) of the Korea Science and Engineering Foundation.

References

[1] R.M. Heck, R.J. Farrauto, Appl. Catal. A: Gen. 221 (2001) 443.
[2] H.S. Gandhi, G.W. Graham, R.W. McCabe, J. Catal. 216 (2003) 433.
[3] J. Barbier Jr., D. Duprez, Appl. Catal. B: Environ. 4 (1994) 105.
[4] A.B.K. Lie, J. Hoebink, G.B. Marin, Chem. Eng. J. 53 (1993) 47.
[5] J. Barbier Jr., D. Duprez, Appl. Catal. B: Environ. 3 (1993) 61.
[6] H. Muraki, S. Matunaga, H. Shinjoh, M.S. Wainwright, D.L. Trimm, J. Chem. Tech. Biotechnol. 52 (1991) 415.
[7] P. Mannila, T. Salmi, H. Haario, M. Luoma, M. Härkönen, J. Sohlo, Appl. Catal. B: Environ. 7 (1996) 179.
[8] J.A. Botas, M.A. Gutiérrez-Ortiz, M.P. González-Marcos, J.A. González-Marcos, J.R. González-Velasco, Appl. Catal. B: Environ. 32 (2001) 243.
[9] S.E. Voltz, C.R. Morgan, D. Liederman, S.M. Jacob, Ind. Eng. Chem. Prod. Res. Dev. 12 (1973) 294.
[10] J.H. Baik, H.J. Kwon, Y.T. Kwon, I.-S. Nam, Se H. Oh, Top. Catal. 42-43 (2007) 337.
[11] H.J. Kwon, J.H. Baik, Y.T. Kwon, I.-S. Nam, S.H. Oh, Chem. Eng. Sci. 62 (2007) 5042.
[12] Se H. Oh, C.C. Eickel, J. Catal. 112 (1988) 543.
[13] S.H. Oh, J. Catal. 124 (1990) 477.
[14] M. Skotak, Z. Karpiński, W. Juszczyk, J. Pielaszek, L. Kepiński, D.V. Kazachkin, V.I. Kovalchuk, J.L. d'Itri, J. Catal. 227 (2004) 11.
[15] A. Martínez-Arias, A.B. Hungría, M. Fernández-García, A. Inglesias-Juez, J.A. Anderson, J.C. Conesa, J. Catal. 221 (2004) 85.
[16] A. Martínez-Arias, M. Fernández-García, A. Inglesias-Juez, A.B. Hungría, J.A. Anderson, J.C. Conesa, J. Soria, Appl. Catal. B: Environ. 31 (2001) 51.
[17] A. Bourane, D. Bianchi, J. Catal. 209 (2002) 126.
[18] A.B. Mhadeswar, D.G. Vlachos, J. Phys. Chem. B 108 (2004) 15246.
[19] G. Socrates, Infrared Characteristic Group Frequencies: Table and Charts, 2nd edition, John Wiley & Sons, 1994.
[20] J. Bergeld, B. Kasemo, D.V. Chakarov, Surf. Sci. 495 (2001) L815.
[21] T.-C. Chang, J.-J. Chen, C.-T. Yeh, J. Catal. 96 (1985) 51.
[22] R. de, S. Monteiro, F.B. Noronha, L.C. Diequez, M. Schmal, Appl. Catal. A: Gen. 131 (1995) 89.
[23] I. Manuel, C. Tomas, H. Colas, N. Matthess, G. Djéga-Mariadassou, Top. Catal. 30/31 (2004) 311.
[24] A. Iglesias-Juez, A. Martínez-Arias, A.B. Hungria, J.A. Anderson, J.C. Conesa, J. Soria, M. Fernández-García, Appl. Catal. A: Gen. 259 (2004) 207.
[25] X. Xu, W. Goodman, J. Phys. Chem. 97 (1993) 7711.
[26] Se H. Oh, G.B. Fisher, J.E. Carpenter, D.W. Goodman, J. Catal. 100 (1986) 360.
[27] B.K. Cho, J. Catal. 138 (1992) 255.
[28] J.H.B.J. Hoebink, R.A. van Gemert, J.A.A. van den Tillaart, G.B. Marin, Chem. Eng. Sci. 55 (2000) 1573.
[29] Y.K. Park, P. Aghalayam, D.G. Vlachos, J. Phys. Chem. A 103 (1999) 8101.
[30] R.K. Herz, S.P. Marin, J. Catal. 65 (1980) 281.
[31] T.H. Fink, J.P. Dath, R. Imbihl, G. Ertl, J. Chem. Phys. 95 (1991) 2109.
[32] D.W. Marquardt, J. Soc. Ind. Appl. Math. 11 (1963) 431.